

# Near-Infrared Light-Emitting Diodes from Organic Radicals with Charge Control

Hwan-Hee Cho, Shun Kimura, Neil C. Greenham, Yuki Tani, Ryota Matsuoka, Hiroshi Nishihara, Richard H. Friend,\* Tetsuro Kusamoto,\* and Emrys W. Evans\*

Organic radicals with fluorescence from doublet-spin energy manifolds circumvent efficiency limits from singlet–triplet photophysics in organic light-emitting diodes (OLEDs). The singly occupied molecular orbital (SOMO) in radicals enables the higher potential performance. The SOMO also presents substantially lower energy frontier orbitals compared to conventional fluorescent emitters for device operation, which can cause severe electron trapping that limits the performance of radical OLEDs. To improve optoelectronic performance, electron donor–acceptor-mixed hosts are used to control charge transport for enhanced radical electroluminescence by charge recombination on SOMO and frontier orbitals. The (2-chloro-3-pyridyl)bis(2,4,6-trichlorophenyl)methyl-based radical is designed to test the charge-controlled device architectures in OLEDs by transient analysis and device characterization studies. Efficient radical OLEDs with 4.7% maximum external quantum efficiency are reported—showing substantial advances in performance for OLEDs with peak emission beyond 800 nm. In addition, substantially improved performance at higher current density operation and more than two orders of higher lifetime stability are achieved with mixed hosts. These results enable pathways to infrared-emitting devices with applications ranging from communications to bioimaging.

several decades since the breakthrough report by Tang et al. in 1987.<sup>[1]</sup> The driver for this research is the chemistry that can be used to design organic emitters with molecular control over their electronic and optical properties in organic light-emitting diodes (OLEDs). An important step was the introduction of highly luminescent platinum- or iridium-based phosphorescent metal complexes, for which OLEDs with an internal quantum efficiency (IQE) of up to 100% were achieved by harvesting 75% normally-dark triplet excitons in addition to 25% singlet excitons formed following electrical excitation.<sup>[2,3]</sup> The substantial enhancement of OLED efficiency and practical performance with phosphorescent emitters has led to commercial devices for red and green pixels in display. There is a motivation to reduce costs using more abundant materials and follow all, organic approaches such as thermally activated delayed fluorescence (TADF), which has emerged as a new technology for next-generation OLEDs.<sup>[4]</sup> To achieve better displays with improved color purity and device stability,


there is also extensive research on TADF or phosphorescent emitters as exciton donors for fluorescent acceptors.<sup>[5,6]</sup>

While there are numerous demonstrations of visible-light emitters based on organic molecules for OLEDs, materials with

## 1. Introduction

Research efforts into molecular organic semiconductors as light emitters in electroluminescent devices have continued over

H.-H. Cho, N. C. Greenham, R. H. Friend  
Cavendish Laboratory  
Department of Physics  
University of Cambridge  
J J Thomson avenue, Cambridge CB3 0HE, UK  
E-mail: rhf10@cam.ac.uk  
S. Kimura, Y. Tani, H. Nishihara  
Department of Chemistry  
Graduate School of Science  
The University of Tokyo  
7-3-1 Hongo, Bunkyo-ku, Tokyo 113-0033, Japan

 The ORCID identification number(s) for the author(s) of this article can be found under <https://doi.org/10.1002/adom.202200628>.

© 2022 The Authors. Advanced Optical Materials published by Wiley-VCH GmbH. This is an open access article under the terms of the Creative Commons Attribution License, which permits use, distribution and reproduction in any medium, provided the original work is properly cited.

DOI: 10.1002/adom.202200628

R. Matsuoka, T. Kusamoto  
Department of Life and Coordination-Complex Molecular Science  
Institute for Molecular Science  
5-1 Higashiyama, Myodaiji, Okazaki, Aichi 444-8787, Japan

R. Matsuoka, T. Kusamoto  
SOKENDAI (The Graduate University for Advanced Studies)  
Shonan Village, Hayama, Kanagawa 240-0193, Japan

H. Nishihara  
Research Center for Science and Technology  
Tokyo University of Science  
2641 Yamazaki, Noda, Chiba 278-8510, Japan

T. Kusamoto  
JST-PRESTO  
4-1-8, Honcho, Kawaguchi, Saitama 332-0012, Japan  
E-mail: kusamoto@ims.ac.jp

E. W. Evans  
Department of Chemistry  
Swansea University  
Singleton Park, Swansea SA2 8PP, UK  
E-mail: emrys.evans@swansea.ac.uk

efficient near-infrared (NIR) emission are less well developed since multi-phonon emission reduces radiative luminescence quantum yields for lower gap organic semiconductors.<sup>[7–9]</sup> However, NIR OLEDs are of interest due to the wide range of technological applications in biosensing, optical imaging, photodynamic therapy, security in personal identification, surveillance, and communications. A variety of emission concepts, such as fluorescence,<sup>[10–12]</sup> phosphorescence,<sup>[13–16]</sup> TADF,<sup>[17–19]</sup> and sensitized fluorescence by TADF or phosphorescence,<sup>[20–22]</sup> have been studied, but the external quantum efficiency (EQE) has not been satisfactory, typically under 5% for emission peak wavelengths of 800 nm and longer.

As a promising alternative, we and others have developed luminescent organic radical materials with doublet emission from 585 to 900 nm.<sup>[23–36]</sup> Organic radicals have unpaired electrons that give rise to doublet spin manifolds, for which we have demonstrated efficient OLEDs with pure-red and mixed red/NIR electroluminescence (EL) from tris(2,4,6-trichlorophenyl)methyl (TTM) radical derivatives.<sup>[34–36]</sup> The high efficiency was attributed to these devices using EL from doublet excitons rather than conventional singlet and triplet excitons that limit the efficiency in standard non-radical devices.

However, high EL efficiency in radical-based OLEDs has only been demonstrated at low current density, and it is important to reduce the efficiency roll-off and turn-on voltage (resulting from poor charge injection), as well as demonstrating operational stability toward practical applications. The radical emitter is typically dispersed at relatively low concentration in a wide-bandgap host, with exciton formation on the emitter taking place by sequential capture of electrons and holes (or vice versa) following injection and transport in the host. Unless the transport of electrons and holes through the emissive layer (EML) is well balanced, recombination will occur in a narrow recombination zone close to the interface with one of the surrounding charge-transport layers. Furthermore, if injection of one carrier into the host is difficult, then direct injection into the small fraction of emitter molecules close to the interface may dominate, also leading to a narrow recombination zone close to the injecting interface. A narrow recombination zone is undesirable since it can lead to bimolecular effects that cause efficiency roll-off at high intensities and promote device degradation. Engineering of the transport and recombination of charges in the EML therefore provides opportunities to enhance device performance.

The most effective and widely used method for improving the balance of electron and hole transport in the EML is to mix electron-transporting and hole-transporting materials in a blended host.<sup>[37–39]</sup> This can be achieved by blending the materials used for the electron- and hole-transport layers (ETL and HTL). Mixed-host approaches have been widely applied not only to fluorescence<sup>[40–42]</sup> and phosphorescence-based devices,<sup>[43–46]</sup> but also with TADF EL,<sup>[47,48]</sup> and TADF- or phosphorescence-sensitized fluorescence.<sup>[49–51]</sup> A further strategy to facilitate control over the recombination zone is to arrange for electron–hole capture to occur primarily in the host followed by energy transfer to the emitter, thus decoupling the recombination process from charge trapping by the emitter.

For efficient and stable NIR OLEDs, we have designed a new NIR emitter based on (3,5-dichloro-4-pyridyl)bis(2,4,6-trichlorophenyl)methyl (PyBTM) radical.<sup>[23]</sup> Triphenylamine-

substituted (2-chloro-3-pyridyl)bis(2,4,6-trichlorophenyl)methyl (PyBTM') (TPA-PyBTM') shows efficient NIR emission around 820 nm and strong absorption between 400 and 550 nm, beneficial for effective Förster resonance energy transfer (FRET). The design of TPA-PyBTM' follows our previously established rules for obtaining emissive  $\pi$ -radicals with non-alternant hydrocarbon motifs (here -TPA and -PyBTM' components). TPA-PyBTM'-based devices were successfully fabricated with maximum external quantum efficiency (EQE) over 4.7%: the highest value of published NIR emissive devices. By exploiting mixed hosts for the radical emitters, improved device charge balance and efficiency roll-off are obtained, here leading to an increase of more than two orders of magnitude in operational lifetime.

## 2. Results and Discussion

The synthesis and characterization of TPA-PyBTM' are shown in the Supporting Information. TPA-PyBTM' is a new NIR radical emitter with energy level features that are suitable for testing radical mixed-host OLEDs, as shown in studies of its spin, electrochemical, photophysical, and quantum-chemical properties. Quantitative electron spin resonance (ESR) spectroscopy confirmed the existence of one unpaired electron for each TPA-PyBTM' molecule. The ESR spectrum displays hyperfine splitting assigned to nitrogen and hydrogen atoms in the PyBTM' moiety indicating delocalization of the spin density over this group (Figure S1a, Supporting Information). Cyclic voltammetry demonstrated two reversible redox waves at  $E'_{\text{red}} = -1.05$  V (vs ferrocenium/ferrocene) and  $E'_{\text{ox}} = 0.15$  V, attributed to reduction centered at the electron-poor PyBTM' moiety and oxidation that removes an electron from the highest occupied molecular orbital (HOMO), a  $\pi$ -orbital delocalized over the electron-rich TPA skeleton and the PyBTM' moiety (Figures S1b and S2, Supporting Information). From this, we estimate singly occupied molecular orbital (SOMO) (reduction) and HOMO energies of 3.8 and 5.0 eV. TPA-PyBTM' displays photoluminescence (PL) in a variety of solvents (Figure S1c and Table S1, Supporting Information) with photoluminescence quantum efficiencies (PLQEs) between 6% and 24%. The peak emission wavelength is redshifted from 742 nm (1.67 eV) to 875 nm (1.42 eV) with increasing solvent polarity, indicating the formation of an intramolecular charge-transfer excited state. These experimental characteristics are supported by density functional theory (DFT) and time-dependent density functional theory (TDDFT) calculations as described in Figure S2 (Supporting Information).

Figure S2 (Supporting Information) shows the calculated molecular orbitals (MOs) of TPA-PyBTM'. The MOs are distributed on both the TPA and the PyBTM' moieties due to the orbital hybridization via efficient  $\pi$ -conjugation. The  $\beta$ -HOMO (184 $\beta$ ) and  $\beta$ -SOMO (185 $\beta$ ) are located mainly at the TPA and the PyBTM' moieties, while their  $\alpha$ -counterparts are delocalized over the entire  $\pi$ -conjugated framework. TDDFT calculation shows that the lowest energy excited state is formed mainly via 185 $\beta$ –184 $\beta$  electronic transition. This transition corresponds to a charge transfer transition from the TPA to the PyBTM' moiety and is assignable to the transition bands observed  $\approx$ 600–750 nm in the absorption spectra. The modeled

charge-transfer character of the doublet excited state is consistent with the solvatochromic effects mentioned above.

TPA-PyBTM' is found to possess a SOMO-HOMO inverted non-Aufbau electronic structure, as deduced from the electrochemical studies and DFT calculations (Figure S2, Supporting Information), but this is not well resolved compared with previous donor-acceptor radicals.<sup>[29,35]</sup> Although SOMO-HOMO inversion is not critical to our application here, it is important that the relatively shallow HOMO energy (5.0 eV) from the electron-rich TPA moiety, and < 1.7 eV doublet exciton energy, sets up properties for TPA-PyBTM' as a new member of donor-acceptor luminescent neutral radicals that can be used for radical EL devices. For excitation harvesting devices with organic radicals, a high HOMO energy is necessary due to the intrinsically low energy, nonbonding type SOMO level ( $\approx 3.7$  eV) that would otherwise drive photoinduced anion formation for radicals.

Figure 1a shows the molecular structures of TPA-PyBTM', 4,4'-bis(carbazol-9-yl)biphenyl (CBP), 4,4',4''-tris(carbazol-9-yl)triphenylamine (TCTA), and bis-4,6-(3,5-di-3-pyridylphenyl)-2-methylpyrimidine (B3PYMPM). The three types of EML composition are designed using these materials, as shown in Figure 1b. For standard devices, CBP is employed as a

conventional host with TPA-PyBTM'. To control charge transport and improve charge balance in the EML, two types of mixed hosts are exploited using typical ETL and HTL materials: B3PYMPM is mixed with CBP to enhance electron transport, and CBP is replaced with TCTA to further increase hole transport. When B3PYMPM is mixed with CBP or TCTA in a 1:1 ratio, emission peaks are observed at 430 nm (CBP:B3PYMPM) and 510 nm (TCTA:B3PYMPM), which are redshifted with respect to the individual host components and indicate exciplex formation (Figure S3, Supporting Information). In this case, it is anticipated that when radical emitters are doped in an exciplex host matrix, both singlet and triplet exciplexes formed on the host can undergo energy transfer to form doublet excitons in the radical dopant for efficient and rapid light emission in EL devices. Direct charge capture on the dopant is also possible.

Figure 2 shows the TPA-PyBTM' steady-state and transient photophysical studies. The PL of CBP, CBP:B3PYMPM, and TCTA:B3PYMPM neat films and the PL and absorption of TPA-PyBTM' diluted in toluene are depicted in Figure 2a. The high absorption coefficient of TPA-PyBTM' between 400 and 550 nm allows the exciplex-forming host to be adopted as an energy donor, and overlap of (exciplex) PL and (radical) absorption enable efficient energy transfer. Values of Förster radius ( $R_0$ )

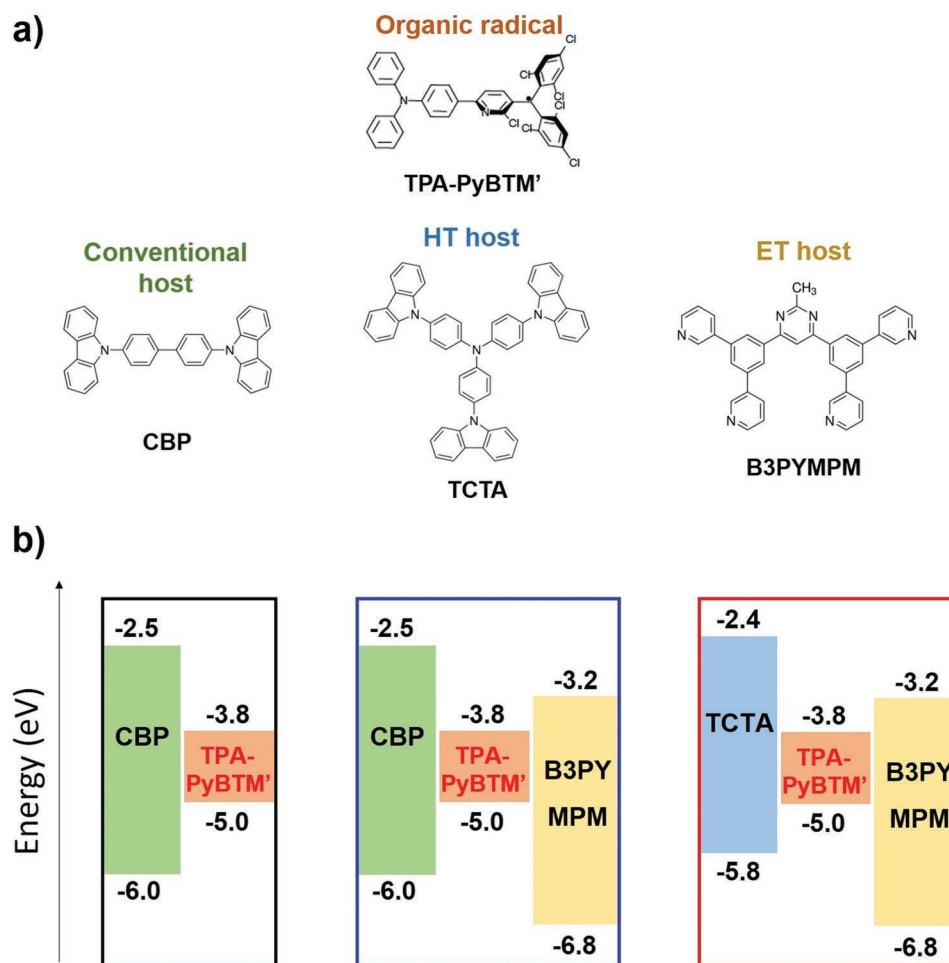


**Figure 1.** a) Chemical structures of TPA-PyBTM', CBP, TCTA, and B3PYMPM. b) Schematic representation of the energy level diagram for the three types of emissive system. CBP is selected for the standard, and B3PYMPM is combined with CBP and TCTA for the mixed hosts with TPA-PyBTM'.

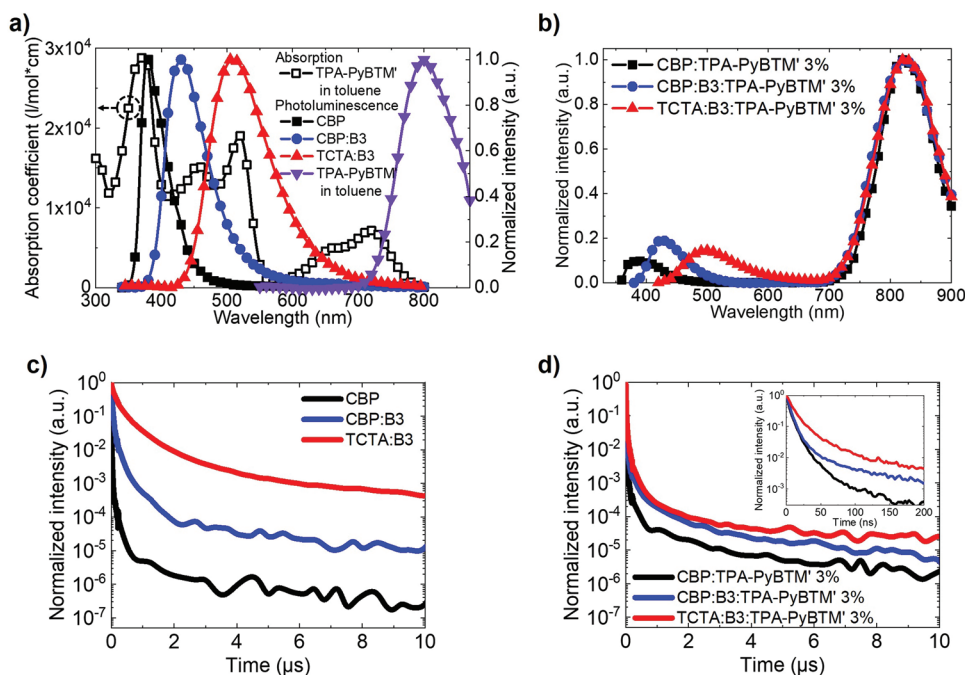


**Figure 2.** Steady-state and transient photophysics. a) PL spectra of CBP, CBP:B3PYMPM, and TCTA:B3PYMPM neat films; and TPA-PyBTM' solution absorption and PL spectra. b) PL spectra of TPA-PyBTM' doped at 3 wt.% in CBP, CBP:B3PYMPM, TCTA:B3PYMPM films. c,d) Transient PL characteristics of CBP, CBP:B3PYMPM, and TCTA:B3PYMPM films and the radical-doped films, respectively. The inset in (d) shows the same data at earlier times.

were calculated for the systems: 3.49, 2.71, and 3.43 nm for TPA-PyBTM' with CBP, CBP:B3PYMPM, and TCTA:B3PYMPM, respectively (with further discussion in the Supporting Information). The steady-state PL spectra of TPA-PyBTM' 3% doped in CBP, CBP:B3PYMPM, and TCTA:B3PYMPM show TPA-PyBTM' emission spectra centered at 820 nm in all cases, with some residual emission contribution from the hosts due to low radical doping concentration (Figure 2b). As the films are excited by a 330 nm laser, NIR emission mainly originates from FRET from the hosts although there is a small contribution by direct excitation of TPA-PyBTM' (Figure S4, Supporting Information). In addition, PLQEs for the TPA-PyBTM'-doped films were measured at the same excitation wavelength as above. The PLQE values for the TPA-PyBTM' 3% doped in CBP:B3PYMPM and TCTA:B3PYMPM films are 14% and 9%, respectively, which is lower than the value of 21% in CBP films.

For the investigation of the excited-state decay kinetics, transient PL measurements were conducted for the three host types with and without TPA-PyBTM' doping, as shown in Figure 2c,d. Characteristic decay timescales were determined from the time-integrated PL intensity (Figure S5, Supporting Information); the time taken for a fraction 1-(1/e) of the total emission to occur are shown in Table S2 (Supporting Information). As expected, due to the reduced oscillator strength, the exciplex emission is slower than the rapid exciton emission seen in CBP. TCTA:B3PYMPM exhibits strong delayed emission in agreement with previous work<sup>[52]</sup> where it was attributed to the formation and recovery of non-emissive triplet exciplex states. CBP:B3PYMPM also shows slow non-monoexponential decay, although the delayed components are not as prominent as in TCTA:B3PYMPM. TPA-PyBTM'-doped films show nanosecond

decay (Figure 2d), with faster emission on all timescales than in the undoped mixed hosts. This implies rapid energy transfer from the singlet exciplex state onto the radical emitter. The decay time for fluorescent doublet emission of TPA-PyBTM' doped in CBP, CBP:B3PYMPM, and TCTA:B3PYMPM are 78, 11.3, and 22.9 ns, respectively. Compared to the radical doped in CBP, the CBP:B3PYMPM and TCTA:B3PYMPM hosted films show longer decay time with delayed components (inset in Figure 2d), which suggests longer time energy transfer from the exciplex formed between CBP or TCTA and B3PYMPM (Figure 2c).

Single-carrier devices were examined to probe charge transport in devices with the different hosts. Figure 3a,b shows the device structures for the hole-only devices (HODs) and electron-only devices (EODs). For the HOD, 1,1-bis[(di-4-tolylamino)phenyl]cyclohexane (TAPC) and TCTA are used as the HTL, and TAPC is inserted between the EML and the cathode to block electron injection into the EML. For the EOD, the EML is sandwiched by the well-established ETL material B3PYMPM to achieve an electron-only current. Figure 3c,d shows the current density-voltage ( $J$ - $V$ ) characteristics of single-carrier devices with and without radical emitter EML doping based on three different hosts: CBP (HOD 1 and EOD 1), CBP:B3PYMPM (HOD 2 and EOD 2), and TCTA:B3PYMPM (HOD 3 and EOD 3). On radical doping, the  $J$ - $V$  curves for both HOD and EOD become shallower in all cases, suggesting that the direct recombination of holes and electrons at the radical sites will dominate the emission mechanism for radical EL. The severe electron trapping (Figure 3d) behavior implies that the emission zone is located close to the EML/ETL interface in full OLED devices. The hole current in HOD 3 is much higher than in other devices

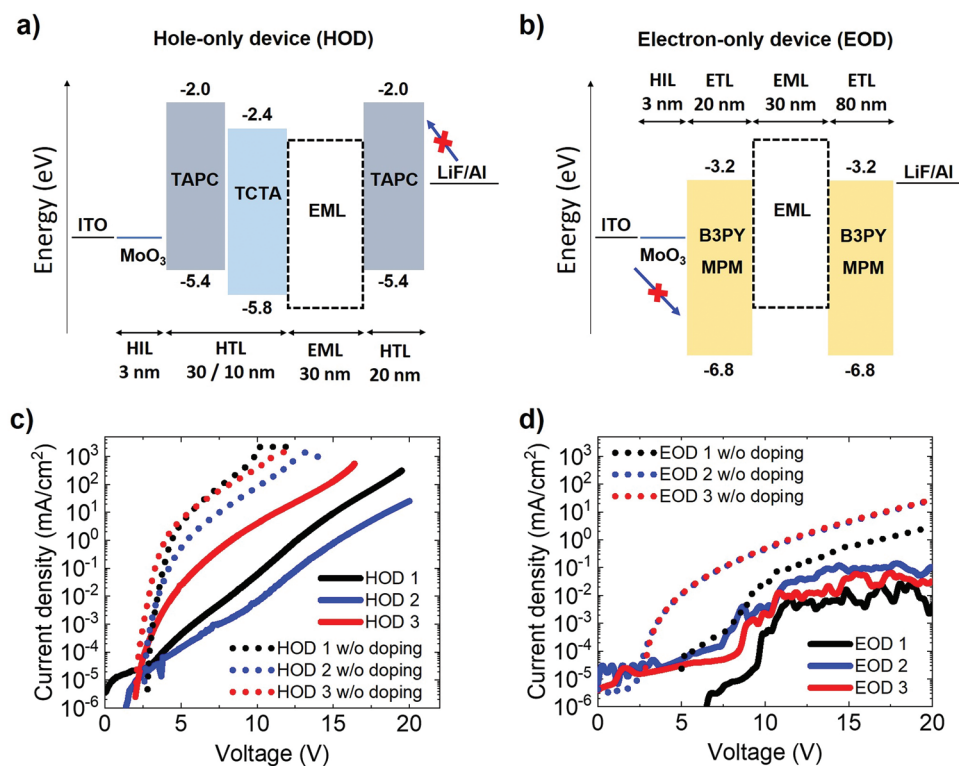


**Figure 3.** a,b) The device architectures of HOD and EOD. For the direct comparison of the hole and electron-transporting properties in devices, the device structures are designed based on usable layers for a full device. Three different hosts were used: CBP (HOD 1 and EOD 1), CBP:B3PYMPM (HOD 2 and EOD 2), and TCTA:B3PYMPM (HOD 3 and EOD 3). For HOD, TAPC 20 nm is used between the EML and cathode to block electron injection. For EOD, B3PYMPM 20 nm is deposited at the anode to allow electron-only currents. c,d) The current density–voltage profiles for the HODs and EODs. As TPA-PyBTM' is doped in the hosts, HOD and EOD plots become shallower, meaning that the radical plays a role in trapping both holes and electrons, but electron trapping is more severe.

due to the improved hole-transporting properties of TCTA compared with CBP,<sup>[53]</sup> and the introduction of B3PYMPM reduces hole transport as observed from the shallower  $J$ – $V$  curve of HOD 2 than HOD 1 (Figure 3c). From EOD studies with and without radical doping, EOD 2 and 3 show steeper  $J$ – $V$  curves than EOD 1, meaning that B3PYMPM considerably improves electron-transporting properties. Enhanced electron transport is apparent despite substantial electron-trapping behavior by the radical dopant SOMO.

Radical EL devices were explored on the basis of the device layout displayed in Figure 4a with EML compositions corresponding to the materials combinations studied above. The three types of devices were successfully characterized, and their performance is shown in Figure 4b–d and Table 1. Figure 4b shows current density–voltage–radiance characteristics. Device 3 exhibits substantially lower turn-on voltage, 2.1 V, than other devices, 2.7 V (Device 1) and 3.3 V (Device 2), which is attributed to the negligible hole injection barrier between HTL and EML as TCTA is used in both layers. Additionally, Device 2 shows 0.6 V higher turn-on voltage than Device 1 as B3PYMPM partially inhibits hole injection to the EML, which is consistent with our HOD studies (Figure 3c).

Figure 4c displays the recorded EQE-current density plots. The maximum EQE of 6.4% was attained from Device 1, with Devices 2 and 3 reaching 4.7% and 3.7%, respectively, and follows the same trend as the film PLQE values: setting

the device efficiency limits for studies of other characteristics such as efficiency roll-off and lifetime. The large efficiency roll-off in Device 1 is mainly ascribed to poor electron transport narrowing the recombination zone, while Devices 2 and 3 exhibit improved efficiency roll-off characteristics, with higher EQEs than Device 1 at current densities over  $1 \text{ mA cm}^{-2}$  since the mixed-host design leads to reduced charge trapping and improved electron transport (Figure 4c; Figure S6, Supporting Information). This is also summarized in Table 1, which shows that at  $10 \text{ mA cm}^{-2}$ , the EQE for Device 1 drops to only 15% of the maximum EQE, while  $\approx 50\%$  and  $40\%$  of the maximum EQE are maintained in Device 2 and 3, respectively.

Figure 4d shows the EL spectra of the devices at  $1 \text{ mA cm}^{-2}$ , where the emission can be seen to peak at wavelengths higher than 800 nm. No host emission is observable, which contrasts with the PL spectra shown in Figure 2b, and suggests that direct electrical excitation of the dopant dominates over possible energy transfer mechanism from host excitons. The EL from Device 1 is slightly blueshifted compared to Device 2 and 3 (not seen in the PL spectra). We infer that this is due to a recombination zone shift.<sup>[54]</sup> Concerning Device 1, the emission zone is close to the EML/ETL interface since the severe electron trapping due to the large energy gap disparity between CBP LUMO and TPA-PyBTM' SOMO is expected from our EOD studies (Figure 3d). In contrast, the recombination zone of Device 2 and 3 can be extended toward the HTL/EML interface because

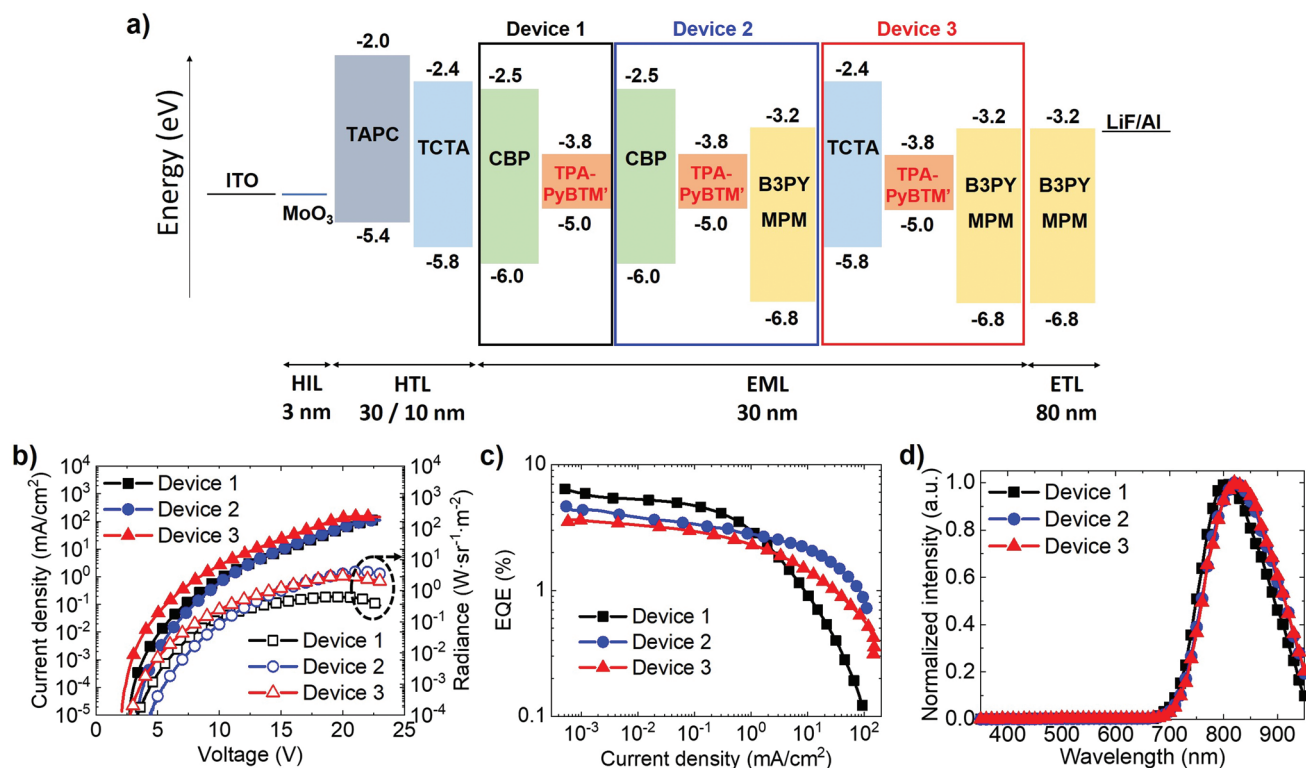


**Figure 4.** Device structures and optoelectronic performance of the TPA-PyBTM' radical-based OLEDs. a) TPA-PyBTM' device layout with energy level diagram for the materials used for this study. b) Current density–voltage–radiance plots. c) EQE–current density curves. d) EL spectra at  $1 \text{ mA cm}^{-2}$ .

of the B3PYMPM's enhanced electron-transporting property, leading to a slight spectrum change compared to Device 1 with increasing optical length from cathode to the emission zone. This can also be supported by the voltage-dependent EL profiles (Figure S7, Supporting Information). Device 1 shows distinct interface exciplex-like emission as voltage increases, indicating that holes and electrons not captured at radical sites are recombined at the interface of EML and ETL. Interface exciplex components are reduced in Device 2 and 3, with much lower contributions even at high voltage ( $>14 \text{ V}$ ). Furthermore, device lifetime was measured at  $1 \text{ mA cm}^{-2}$  ( $10.3 \text{ V}$  for Device 1,  $10.7 \text{ V}$  for Device 2, and  $8.4 \text{ V}$  for Device 3) for the devices (Figure S8, Supporting Information). As we have investigated, the mixed hosts are conducive to more balanced charge populations in an extended recombination zone; this results in substantially improved device stability ( $70 \text{ s}$  for Device 1,  $3.4 \text{ h}$  for Device 2, and  $0.5 \text{ h}$  for Device 3). The approximately seven times shorter lifetime of Device 3 than Device 2 is attributed to the higher hole mobility and shallower HOMO energy level in TCTA

compared to CBP, leading to reduced hole trapping at radical dopant sites and hole accumulation at the EML/ETL interface for increased exciton–polaron quenching.<sup>[37,38]</sup> Additionally, it is noted that as lifetime was measured at relatively high voltage in an ambient condition without encapsulation, the absolute device lifetime could be enhanced in more optimized device configurations and measurement conditions.

### 3. Conclusion

In conclusion, efficient NIR OLEDs were successfully demonstrated by combining novel radical emitters with mixed hosts for improved device characteristics. The high absorption coefficient of TPA-PyBTM' in the range of  $400\text{--}550 \text{ nm}$  allows efficient transfer from the energy donor to the radical as an energy acceptor. We demonstrated that improvement in charge balance of holes and electrons with the extended emission zone enables more stable devices with improved efficiency roll-off.

**Table 1.** Summary of Device Performance.

	$V_{\text{on}}^{\text{a}}$ [V]	$\text{EQE}_{\text{Max}}^{\text{b}}$ [%]	$\text{EQE}_{\text{J-1.0}}^{\text{b}}$ [%]	$\text{EQE}_{\text{J-10.0}}^{\text{c}}$ [%]	$\text{Radiance}_{\text{Max}} [\text{W sr}^{-1} \text{m}^{-2}]$	$\lambda_{\text{max}}$ [nm]
Device 1	2.7	6.4	3.0	0.9	0.6	805
Device 2	3.3	4.7	2.8	2.2	4.0	820
Device 3	2.1	3.7	2.3	1.4	3.0	820

<sup>a</sup>) Voltage at  $10^{-5} \text{ mA cm}^{-2}$ ; <sup>b</sup>) EQE at  $1 \text{ mA cm}^{-2}$ ; <sup>c</sup>) EQE at  $10 \text{ mA cm}^{-2}$

From conventional charge-trapping-type devices, we achieved a maximum EL EQE of 6.4%, and with mixed hosts, we could not only improve the efficiency roll-off but also found substantially better device lifetimes, more than one hundred times longer than conventional devices. The slightly reduced EQE values with mixed hosts could be improved with more optimized mixed-host combinations in future work. However, the low-lying nature of the functional SOMO and HOMO energy levels of the radical leads to the requirement of electron transport materials having lower energy levels with high electron mobility than typically used for non-radical dopants in optoelectronics. This limits the range of suitable candidates from the established materials and indicates a necessity for research on new materials to unlock the full potential of the device strategy presented here. Our results indicate a pathway for radical-based optoelectronic devices with doublet emission for infrared light-emitting technologies with diverse applications from security and communications to biomedical sensing.

## 4. Experimental Section

**Synthesis, Characterization, and Calculations of TPA-PyBTM'**: The details are described in the Supporting Information.

**Sample Preparation**: To measure PL and absorption spectra in solution, TPA-PyBTM' was dissolved in toluene with 0.2 mg ml<sup>-1</sup>. Organic films were made by a thermal evaporation process under high vacuum ( $\approx 10^{-7}$  torr). Fifty nanometers films of CBP, CBP:B3PYMPM, TCTA:B3PYMPM and TPA-PyBTM' 3 wt.% doped in CBP, CBP:B3PYMPM, and TCTA:B3PYMPM were deposited on glass substrates to measure steady-state PL, PLQE, and transient PL. Mixed films were prepared by controlled evaporation from separate crucibles for each material. For the fabrication of OLEDs and single-carrier devices, ITO coated substrates ( $\approx 15 \Omega \text{ cm}^{-2}$ ) were cleaned with acetone and isopropyl alcohol, and then O<sub>2</sub> plasma treatment was applied to align the energy level with a hole transporting layer. All layers, including organic layers and a LiF/aluminum cathode, were thermally deposited under high vacuum ( $\approx 10^{-7}$  torr).

**Photophysical Measurements**: Steady-state PL spectra were measured by an Edinburgh Instruments fluorescence spectrometer (FLS980) with a monochromated xenon arc lamp at  $\lambda_{\text{ex}} = 330 \text{ nm}$  under a nitrogen flow. Shimadzu UV-3600 Plus spectrophotometer was employed for the measurement of absorption spectra. FLS980 with an integrating sphere under a nitrogen flow was used to measure PLQE, and the films were excited by 330 nm laser. Transient PL was recorded by using an Andor electrically gated intensified charge-coupled device (ICCD) with 330 nm laser excitation; the decay kinetics were obtained from the integration of the total spectrum at each time.

**Device Characterization**: The *J-V* characteristics of single-carrier devices were recorded by a Keithley 2635 source-meter. The performance of the OLED devices was measured by a Keithley 2635 source-meter and a calibrated Si photodiode. The EL spectra were recorded by an Ocean Optics Flame spectrometer.

## Supporting Information

Supporting Information is available from the Wiley Online Library or from the author.

## Acknowledgements

This work was supported by the Engineering and Physical Sciences Research Council (EPSRC, grant no. EP/M005143/1). EE acknowledges

funding from the Royal Society for University Research Fellowship (URF/R1/201300). This project has received funding from the ERC under the European Union's Horizon 2020 Research and Innovation Programme (grant agreement number 101020167). HC acknowledges George and Lilian Schiff Foundation for Ph.D. studentship funding. The present study was partly supported by JST PRESTO (grant no. JPMJPR20L4) and JSPS KAKENHI (grant no. JP20H02759).

## Conflict of Interest

The authors declare no conflict of interest.

## Data Availability Statement

The data underlying this article are available at: 10.6084/m9.figshare.20411271.

## Keywords

energy transfer, mixed hosts, near-infrared organic light-emitting diodes, organic radicals

Received: March 28, 2022

Revised: June 29, 2022

Published online: August 21, 2022

- [1] C. W. Tang, S. A. VanSlyke, *Appl. Phys. Lett.* **1987**, *51*, 913.
- [2] C. Adachi, M. A. Baldo, M. E. Thompson, S. R. Forrest, *J. Appl. Phys.* **2001**, *90*, 5048.
- [3] M. A. Baldo, D. F. O'Brien, Y. You, A. Shoustikov, S. Sibley, M. E. Thompson, S. R. Forrest, *Nature* **1998**, *395*, 151.
- [4] H. Uoyama, K. Goushi, K. Shizu, H. Nomura, C. Adachi, *Nature* **2012**, *492*, 234.
- [5] M. A. Baldo, M. E. Thompson, S. R. Forrest, *Nature* **2000**, *403*, 750.
- [6] H. Kaji, H. Suzuki, T. Fukushima, K. Shizu, K. Suzuki, S. Kubo, T. Komino, H. Oiwa, F. Suzuki, A. Wakamiya, Y. Murata, C. Adachi, *Nat. Commun.* **2015**, *6*, 8476.
- [7] A. Zampetti, A. Minotto, F. Cacialli, *Adv. Funct. Mater.* **2019**, *29*, 1807623.
- [8] F. C. Spano, C. Silva, *Annu. Rev. Phys. Chem.* **2014**, *65*, 477.
- [9] R. Englman, J. Jortner, *Mol. Phys.* **1970**, *18*, 145.
- [10] D. Baigent, P. Hamer, R. H. Friend, S. Moratti, A. Holmes, *Synth. Met.* **1995**, *71*, 2175.
- [11] P. Murto, A. Minotto, A. Zampetti, X. Xu, M. R. Andersson, F. Cacialli, E. Wang, *Adv. Opt. Mater.* **2016**, *4*, 2068.
- [12] A. Minotto, P. Murto, Z. Genene, A. Zampetti, G. Carnicella, W. Mammo, M. R. Andersson, E. G. Wang, F. Cacialli, *Adv. Mater.* **2018**, *30*, 1706584.
- [13] K. R. Graham, Y. Yang, J. R. Sommer, A. H. Shelton, K. S. Schanze, J. Xue, J. R. Reynolds, *Chem. Mater.* **2011**, *23*, 5305.
- [14] J. Xue, L. Xin, J. Hou, L. Duan, R. Wang, Y. Wei, J. Qiao, *Chem. Mater.* **2017**, *29*, 4775.
- [15] J. R. Sommer, R. T. Farley, K. R. Graham, Y. Yang, J. R. Reynolds, J. Xue, K. S. Schanze, *ACS Appl. Mater. Interfaces* **2009**, *1*, 274.
- [16] Y.-C. Wei, S. F. Wang, Y. Hu, L.-S. Liao, D.-G. Chen, K.-H. Chang, C.-W. Wang, S.-H. Liu, W.-H. Chan, J.-L. Liao, W.-Y. Hung, T.-H. Wang, P.-T. Chen, H.-F. Hsu, Y. Chi, P.-T. Chou, *Nat. Photonics* **2020**, *14*, 570.
- [17] D. H. Kim, A. D'Aléo, X. K. Chen, A. D. S. Sandanayaka, D. Yao, L. Zhao, T. Komino, E. Zaborova, G. Canard, Y. Tsuchiya, E. Choi,

- J. W. Wu, F. Fages, J. L. Brédas, J. C. Ribierre, C. Adachi, *Nat. Photonics* **2018**, 12, 98.
- [18] Y. Yuan, Y. Hu, Y.-X. Zhang, J.-D. Lin, Y.-K. Wang, Z.-Q. Jiang, L.-S. Liao, S.-T. Lee, *Adv. Funct. Mater.* **2017**, 27, 1700986.
- [19] S. Wang, X. Yan, Z. Cheng, H. Zhang, Y. Liu, Y. Wang, *Angew. Chem., Int. Ed.* **2015**, 54, 13068.
- [20] J. Brodeur, L. Hu, A. Malinge, E. Eizner, W. G. Skene, S. Kéna-Cohen, *Adv. Opt. Mater.* **2019**, 7, 1901144.
- [21] A. Shahalizad, A. Malinge, L. Hu, G. Laflamme, L. Haeberlé, D. M. Myers, J. Mao, W. G. Skene, S. Kéna-Cohen, *Adv. Funct. Mater.* **2020**, 31, 2007119.
- [22] T. Liu, G. Xie, C. Zhong, S. Gong, C. Yang, *Adv. Funct. Mater.* **2018**, 28, 1706088.
- [23] Y. Hattori, T. Kusamoto, H. Nishihara, *Angew. Chem., Int. Ed.* **2014**, 126, 12039.
- [24] A. Abdurahman, Y. Chen, X. Ai, O. Ablikim, Y. Gao, S. Dong, B. Li, B. Yang, M. Zhang, F. Li, *J. Mater. Chem. C* **2018**, 6, 11248.
- [25] S. Dong, W. Xu, H. Guo, W. Yan, M. Zhanga, F. Li, *Phys. Chem. Chem. Phys.* **2018**, 20, 18657.
- [26] A. Heckmann, S. Dümmmler, J. Pauli, M. Margraf, J. Köhler, D. Stich, C. Lambert, I. Fischer, U. Resch-Genger, *J. Phys. Chem. C* **2009**, 113, 20958.
- [27] Y. Hattori, T. Kusamoto, H. Nishihara, *RSC Adv.* **2015**, 5, 64802.
- [28] Y. Hattori, E. Michail, A. Schmiedel, M. Moos, M. Holzapfel, I. Krummenacher, H. Braunschweig, U. Meller, J. Pflaum, C. Lambert, *Chem. - Eur. J.* **2019**, 25, 15463.
- [29] A. Tanushi, S. Kimura, T. Kusamoto, M. Tominaga, Y. Kitagawa, M. Nakano, H. Nishihara, *J. Phys. Chem. C* **2019**, 123, 4417.
- [30] Z. Cui, S. Ye, L. Wang, H. Guo, A. Obolda, S. Dong, Y. Chen, X. Ai, A. Abdurahman, M. Zhang, L. Wang, F. Li, *J. Phys. Chem. Lett.* **2018**, 9, 6644.
- [31] D. Velasco, S. Castellanos, M. López, F. López-Calahorra, E. Brillas, L. Julia, *J. Org. Chem.* **2007**, 72, 7523.
- [32] S. Castellanos, D. Velasco, F. López-Calahorra, E. Brillas, L. Julia, *J. Org. Chem.* **2008**, 73, 3759.
- [33] Q. Peng, A. Obolda, M. Zhang, F. Li, *Angew. Chem., Int. Ed.* **2015**, 54, 7091.
- [34] X. Ai, E. W. Evans, S. Dong, A. J. Gillett, H. Guo, Y. Chen, T. J. H. Hele, R. H. Friend, F. Li, *Nature* **2018**, 563, 536.
- [35] H. Guo, Q. Peng, X.-K. Chen, Q. Gu, S. Dong, E. W. Evans, A. J. Gillett, X. Ai, M. Zhang, D. Credginton, V. Coropceanu, R. H. Friend, J.-L. Brédas, F. Li, *Nat. Mater.* **2019**, 18, 977.
- [36] A. Abdurahman, T. J. H. Hele, Q. Gu, J. Zhang, Q. Peng, M. Zhang, R. H. Friend, F. Li, E. W. Evans, *Nat. Mater.* **2020**, 19, 1224.
- [37] C. Murawski, K. Leo, M. C. Gather, *Adv. Mater.* **2013**, 25, 6801.
- [38] S. Scholz, D. Kondakov, B. Lüssem, K. Leo, *Chem. Rev.* **2015**, 115, 8449.
- [39] H. Aziz, Z. D. Popovic, N.-X. Hu, A.-M. Hor, G. Xu, *Science* **1999**, 283, 1900.
- [40] J.-H. Lee, C.-I. Wu, S.-W. Liu, C.-A. Huang, Y. Chang, *Appl. Phys. Lett.* **2005**, 86, 103506.
- [41] S. W. Liu, C. A. Huang, J. H. Lee, K. H. Yang, C. C. Chen, Y. Chang, *Thin Solid Films* **2004**, 453, 312.
- [42] A. B. Chwang, R. C. Kwong, J. J. Brown, *Appl. Phys. Lett.* **2002**, 80, 725.
- [43] Y.-S. Park, S. Lee, K.-H. Kim, S.-Y. Kim, J.-H. Lee, J.-J. Kim, *Adv. Funct. Mater.* **2013**, 23, 4914.
- [44] N. Chopra, J. S. Swensen, E. Polikarpov, L. Cosimbescu, F. So, A. B. Padmaperuma, *Appl. Phys. Lett.* **2010**, 97, 033304.
- [45] M. E. Kondakova, T. D. Pawlik, R. H. Young, D. J. Giesen, D. Y. Kondakov, C. T. Brown, J. C. Deaton, J. R. Lenhard, K. P. Klubek, *J. Appl. Phys.* **2008**, 104, 094501.
- [46] J. Lee, J.-I. Lee, J. Y. Lee, H. Y. Chu, *Appl. Phys. Lett.* **2009**, 94, 193305.
- [47] C.-K. Moon, K. Suzuki, K. Shizu, C. Adachi, H. Kaji, J.-J. Kim, *Adv. Mater.* **2017**, 29, 1606448.
- [48] J. W. Sun, J.-H. Lee, C.-K. Moon, K.-H. Kim, H. Shin, J.-J. Kim, *Adv. Mater.* **2014**, 26, 5684.
- [49] D. Li, Y. Hua, L.-S. Liao, *J. Mater. Chem. C* **2019**, 7, 977.
- [50] H.-G. Kim, K.-H. Kim, C.-K. Moon, J.-J. Kim, *Adv. Opt. Mater.* **2017**, 5, 1600749.
- [51] H.-G. Kim, K.-H. Kim, J.-J. Kim, *Adv. Mater.* **2017**, 29, 1702159.
- [52] Y.-S. Park, K.-H. Kim, J.-J. Kim, *Appl. Phys. Lett.* **2013**, 102, 153306.
- [53] X. Zhang, X. Guo, Y. Chen, J. Wang, Z. Lei, W. Lai, Q. Fan, W. Huang, *J. Lumin.* **2015**, 161, 300.
- [54] C.-H. Hsiao, Y.-H. Chen, T.-C. Lin, C.-C. Hsiao, J.-H. Lee, *Appl. Phys. Lett.* **2006**, 89, 163511.